



# Field tests and numerical analysis of the effects of scour on a full-scale soil–foundation–structural system

Enrico Tubaldi<sup>1</sup> · Christos Antonopoulos<sup>1</sup> · Stergios Aristoteles Mitoulis<sup>2</sup> · Sotirios Argyroudis<sup>3</sup> · Fabrizio Gara<sup>4</sup> · Laura Ragni<sup>4</sup> · Sandro Carbonari<sup>4</sup> · Francesca Dezi<sup>5</sup> · Athanasios Vratsikidis<sup>6</sup> · Dimitris Pitilakis<sup>6</sup> · Anastasios Anastasiadis<sup>6</sup>

Received: 24 March 2022 / Revised: 13 June 2022 / Accepted: 11 July 2022  
© The Author(s) 2022

## Abstract

Scour is the prevailing cause of bridge failure worldwide, leading not only to traffic disruption, but also to social and economic losses and even to casualties. Many vibration-based monitoring techniques have been proposed for identifying the scour location and extent, based on the evaluation of the changes of the bridge modal properties due to scour. This study describes the experimental and numerical research carried out to investigate the effects of scour on the dynamic properties of structures with shallow foundations. Although these are the most vulnerable ones, they have received less attention compared to structures founded on pile foundations. To fill some existing knowledge gaps, field experiments were carried out on EuroProteas, a structural prototype with shallow foundation that was subjected to increasing levels of scour. The changes of the dynamic properties of the system are evaluated by postprocessing the ambient vibration recordings and by developing various models of the soil–foundation–structural system with different descriptions of the soil–structure interaction problem. The study results shed light on the effects of scour on systems with shallow foundations and on the accuracy of alternative modelling approaches. They are presented here to inform the development and validation of vibration-based techniques and modelling strategies for bridge scour identification.

**Keywords** Bridge scour · Field test · Soil–structure interaction · Ambient vibrations · Vibration-based identification · Structural health monitoring

## 1 Introduction

Bridge scour, namely, the removal of sediments surrounding underwater foundations due to water flow and turbulence [1, 2] is the leading cause of bridge failure worldwide. Exacerbated by climate change effects [3], this phenomenon induces considerable fatalities, traffic disruption, and significant economic and societal losses [4, 5]. Scour has two main

effects on bridges: decreased stiffness of the soil–foundation–structure (SFS) system and reduction of foundation carrying capacity. Many types of bridges, such as masonry-arch or multi-span bridges, have shallow foundations and are very vulnerable to scour [6], which often worsens with time due to the accumulation of this effect under multiple floods [7, 8] and/or multiple independent hazards such as the occurrence of an earthquake that hits a bridge with scoured foundations [9, 10]. New bridges usually have deep foundations, making them less vulnerable and hence more resilient to scour. However, even for these bridges, the foundation scour may result in changes of the boundary conditions, which modify their global stiffness and eventually decrease their capability to withstand both vertical and lateral loadings [11].

Understanding the complex interaction between the continuously evolving scour process and the dynamic behaviour of the affected bridges is of paramount importance for the development of low-cost, non-invasive monitoring strategies aimed at indirectly evaluating scour by measuring the

✉ Christos Antonopoulos  
christos.antonopoulos@strath.ac.uk

<sup>1</sup> University of Strathclyde, Glasgow, UK

<sup>2</sup> infrastructuResilience, London, UK

<sup>3</sup> Brunel University London, London, UK

<sup>4</sup> Università Politecnica delle Marche, Ancona, Italy

<sup>5</sup> University of Camerino, Camerino, Italy

<sup>6</sup> Aristotle University of Thessaloniki, Thessaloniki, Greece

changes in bridge modal properties [12]. In fact, it is well known that relying entirely on underwater visual inspections for quantifying the risk of a bridge collapse due to scour is not recommended, due to a series of limitations, the main one being that inspections cannot be carried out during the peak of the flood event, when the scour risk is maximum [13, 14]. At the same time, the use of sensors to measure the scour depth directly (e.g., with scour probes) can also be problematic, due to the high costs of sensors and more importantly the difficulties in installing them, obtaining permission from, e.g., environmental agencies, county councils, and planning authorities [15].

For these reasons, there are many studies in the literature that investigate the possibility of identifying the scour location and extent by means of vibration-based monitoring techniques, based on the evaluation of the changes of the bridge modal properties due to scour. Briaud et al. [16] focused on the use of accelerometers and tiltmeters to monitor scour, and carried out experiments on two large scale laboratory models with shallow and deep foundations. Subsequently, two individual monitoring systems were designed and installed on two real bridges. The results of the experimental campaigns showed that the instruments could be successfully employed to provide warnings of potential bridge failure. However, there were shortcomings with regard to the accelerometers, which are related to lack of sufficient excitation from traffic and the high-power consumption required for the transmission of accelerometer data, for which typical solar panel and battery are not sufficient. Another study by Prendergast et al. [17] focused on single cantilever piles with the bottom part embedded in the soil, excited by a top impulse force, and on the development of a finite element model for capturing the effects of scour. The study showed that the effect of water on the measured natural frequencies of the cantilevers is negligible. Bao et al. [18] conducted similar experiments for vibration-based monitoring of scour and investigated the effect of the scour hole shape. This is usually assumed as symmetric in experiments, whereas in reality, it has often a non-symmetric shape [6]. The experiments with unsymmetrical scour hole scenarios carried out in [18] demonstrated the importance of this factor for vibration-based scour detection. Foti and Sabia [19] proposed and evaluated two alternative techniques for monitoring foundation scour using measurements of traffic-induced vibrations. Similarly, Prendergast et al. [20] investigates the local sensitivity to scour of the vibration modes of a bridge, using a vehicle–bridge–soil dynamic interaction model for identifying both the occurrence and the location of the scour. Bao and Liu [21] developed a formula for predicting the predominant natural frequency of bridge piers under future higher scour widths by measuring only the response under a few small scour widths. Other recent numerical and experimental

studies have been carried out on the use of ambient vibration recordings for scour identification [22–25].

Even though many studies have investigated numerically and experimentally the changes of the dynamic behaviour of bridges with deep foundations subjected to scour, it is surprising that research on bridges with shallow foundations is scarce. This is probably because very often the simple problem of scour of a single monopile pier-system with circular diameter is considered in experimental flume studies on scour development and in studies investigating the changes of the dynamic properties of bridges. For this reason, there are not many studies investigating the geometry of the scour hole in case of pier on shallow foundations, with the exception of the recent work of Lee et al. [26]. As a result of this, many numerical and experimental studies investigating the effects of scour on bridges with shallow foundations introduced some simplifications in the description of scour (see, e.g., [27–29]). They also assumed scour profiles that are more representative of degradation scour rather than local scour, which is more critical for bridges.

However, the scour effect is indeed more pronounced or critical for bridges with shallow foundation compared to deep foundations, and thus more attention should be paid on this issue. Scour affects significantly the bearing capacity of the foundation resulting, in some occasions, in tilting, and subsequently in bridge damage, failure and collapse either during the event or over time [30, 31]. The soil erosion around the foundation prevents the loading from the bridge to be transferred into the ground leading to a bridge instability.

Guo [32] analysed numerically the changes of shallow foundation impedances due to foundation scour, highlighting the reduction of foundation stiffness and radiation damping, and evaluating the effects on the dynamic performance. Experimental tests were carried out by Ruocci et al. [33] by imposing increasing levels of scour and applying damage detection techniques on a 1/2 scale model of a two-span bridge. Malekjafarian et al. [29] developed an approach to detect the vertical stiffness loss of multi-span bridges with shallow foundations due to scour based monitoring relative changes in vertical pier-mode shape amplitudes by means of recorded acceleration signals. Particularly, a scour monitoring indicator was proposed to compare the mode shape value of a given pier with those at the other piers. Kariyawasam et al. [28] carried out experimental centrifuge tests on a scaled bridge with shallow foundations to investigate the sensitivity of its natural frequency to scour, considering symmetric or triangular scour hole shapes that allow to treat the problem as a two-dimensional one, while local scour calls for the use of three-dimensional models. Scozzese et al. [34] studied the case of Rubbianello bridge, a multi-span masonry arch bridge with shallow foundations located in

Central Italy, which suffered a partial collapse due to scour. They developed a three-dimensional model of the bridge, and simulated the development of a local scour hole shape at the base of a pier. They concluded that significant variations of modal properties occur only after the excavation reaches the foundation base and that monitoring the changes of vibration frequency may not provide sufficient warning of the risk of collapse due to scour for this type of bridges.

From the analysis of the literature of the problem, it is evident that most experimental studies on shallow foundations have been carried out in the laboratory, under controlled conditions, where it is impossible to fully recreate in-field conditions. As a consequence of this, there is also a lack of fully validated numerical strategies for simulating the effect of scour on the dynamic behaviour of soil–foundation–structure systems subjected to scour. Thus, further experimental and numerical research investigations on the problem are needed. The DYMOBRIS EU project [35] was conceived with the objective of contributing to fill the knowledge gap in experimental evaluation and modelling of the effects of scour on systems with shallow foundations, which are the most vulnerable to scour. For this purpose, full-scale free and forced-vibration tests and recordings of ambient vibrations signals were carried out on the EuroProteas prototype [36, 37] at EuroseisTest in June, 2019 to evaluate the effects of foundation scour on the dynamic properties of a SFS system. The experimental tests have been complemented by

numerical analyses, aimed to validate the numerical modelling strategies for describing the effects of scour on the dynamic behaviour of the SFS system.

Section 2 describes the field test setup at EuroProteas and the investigated scour scenarios. Section 3 illustrates various modelling strategies developed to analyse the variation of dynamic properties of the in-field prototype due to scour, based on different description of the soil–structure interaction problem. Section 4 illustrates the ambient vibration test results and compares them with those obtained by the numerical models. Finally, Sect. 5 shows the updating of the numerical model to provide a better interpretation of the test results. It is noteworthy that the study results are useful not only for the development of vibration-based monitoring strategies for bridge scour, but they also contribute to improve the understanding of the effect of scour on the dynamic impedance of bridge foundations undergoing scour. This is of paramount importance for investigating the seismic response of bridges with scoured shallow foundation, which has received increased attention in the literature in the last decade [38–42].

## 2 Field test setup

EuroProteas (Fig. 1) is a double symmetric prototype structure, which simply rests on the ground surface. Its superstructure mass consists of two portable reinforced concrete

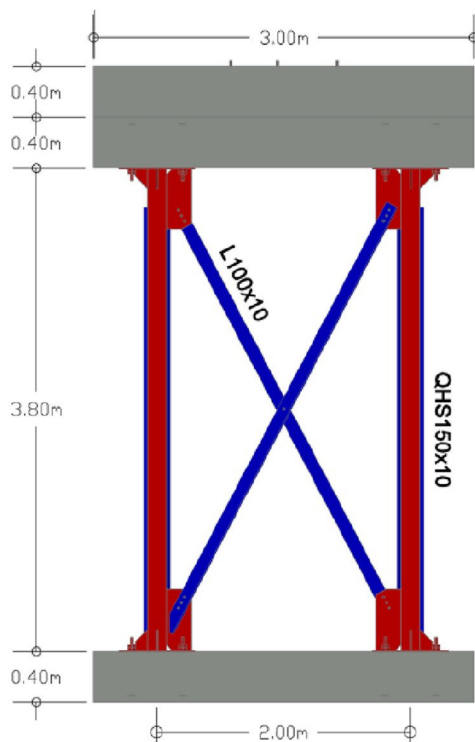


Fig. 1 Geometry and characteristics of EuroProteas [36]

slabs, bolted on four square hollow steel columns connected by steel X-braces. An identical reinforced concrete slab is used as a surface foundation of the model. The reconfigurable roof mass and bracing system allow achieving different values of the fixed base natural frequency of the structure and of the superstructure to soil stiffness ratio. The slabs mentioned above with dimensions  $3.0 \times 3.0 \times 0.4$  m are made of concrete C20/25 and steel reinforcement of diameter 14 mm. The unit weight of the reinforced concrete is  $25 \text{ kN/m}^3$ , leading to a mass of around 9.16 Mg for each slab. The four steel columns have cross sections QHS  $150 \times 150 \times 10$  mm, length 3.8 m, and a total mass of approximately 0.68 Mg, while the X-braces have L cross sections  $100 \times 100 \times 10$  mm and a total mass of approximately 0.41 Mg. The steel columns are fixed to the slabs using M20 steel bolts. The braces are conjoined to each other and to steel plates welded on the base of the columns by M16 bolts. The total height of EuroProteas is 5 m, whereas its total mass is approximately 28.5 Mg.

The considered prototype can provide a simplified representation of a stiff bridge pier of a multi-span simply supported deck, such that the deck does not contribute to the lateral stiffness of the system (Fig. 2). It would have been more realistic to consider alternative prototypes with geometrical and mechanical properties matching the ones of real bridges. This study is characterised by potential limitations, namely, the relatively high ratio of the foundation mass to superstructure mass, the presence of solely granular soil under the foundation, and hence the consideration of drain conditions, and finally the absence of water in the field, which provides a contribution in terms of inertia and loads on submerged bridge piers. However, the main scope of this study is to validate numerical strategies for simulating the effect of scour on the dynamic properties of systems with the aid of large-scale field test results. Thus, the strategies developed, once validated, can be used to analyse other structures. The development of such a modelling strategy is essential for interpreting the results of any vibration-based monitoring strategy for scour measurement.

## 2.1 Soil properties

EuroProteas is built at EuroSeisTest experimental facility, whose soil and dynamic properties have been investigated thoroughly by earlier studies through comprehensive geotechnical and geophysical surveys [43]. Recently, Pitilakis et al. [36] carried out an array of additional geotechnical and geophysical field tests (drilling boreholes, down-hole measurements, and resonant column tests on representative soil specimens) to identify the exact soil conditions beneath EuroProteas. Laboratory tests were carried out for specimens from various depths and locations beneath the foundation providing detailed and valuable data before the construction of EuroProteas. Notably, a 12 m deep borehole (denoted as “BH-01”) was drilled at the eastern side of EuroProteas at a distance of 0.5 m of the foundation, while a 30 m deep borehole (denoted as “BH-02”) was drilled beneath the geometrical center of the foundation.

Figure 3 illustrates a comprehensive 30 m stratigraphy derived by the BH-02 and the low-strain shear wave velocity profile obtained by a down-hole test (denoted as “DH-01”) along with other  $V_s$  profiles in EuroProteas vicinity [44–46]. For the sake of completeness, the  $N_{\text{SPT}}$  profile corresponding to BH-02 is also provided. According to the data provided by the BH-02 (Fig. 3), the top 7 m (unit A) of the soil consists mainly of silty clayey with sand, whereas for depths 7–22 m (unit B) and 22–30 m (unit C) of silty sand with gravels to clayey sand and of silty sand, respectively. Moreover,  $N_{\text{SPT}}$  does not exceed 6 in the upper 6 m, and the water level was found at 1.7 m below ground surface. Shear wave velocity ranges from 100 to 130 m/s in the upper 5 m and exceeds 300 m/s at 25 m depth.

## 2.2 Sensor types and arrangement

Figure 4 shows the instrumentation installed on EuroProteas. Three triaxial accelerometers were placed on the roof slab, while another four triaxial accelerometers are placed on the top of the foundation slab (Table 1). All the accelerometers were oriented toward the positive  $x$ -direction of the

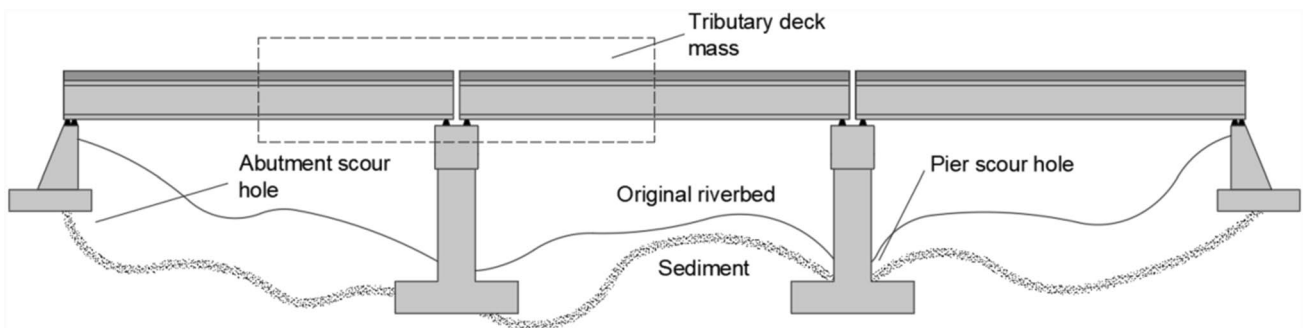
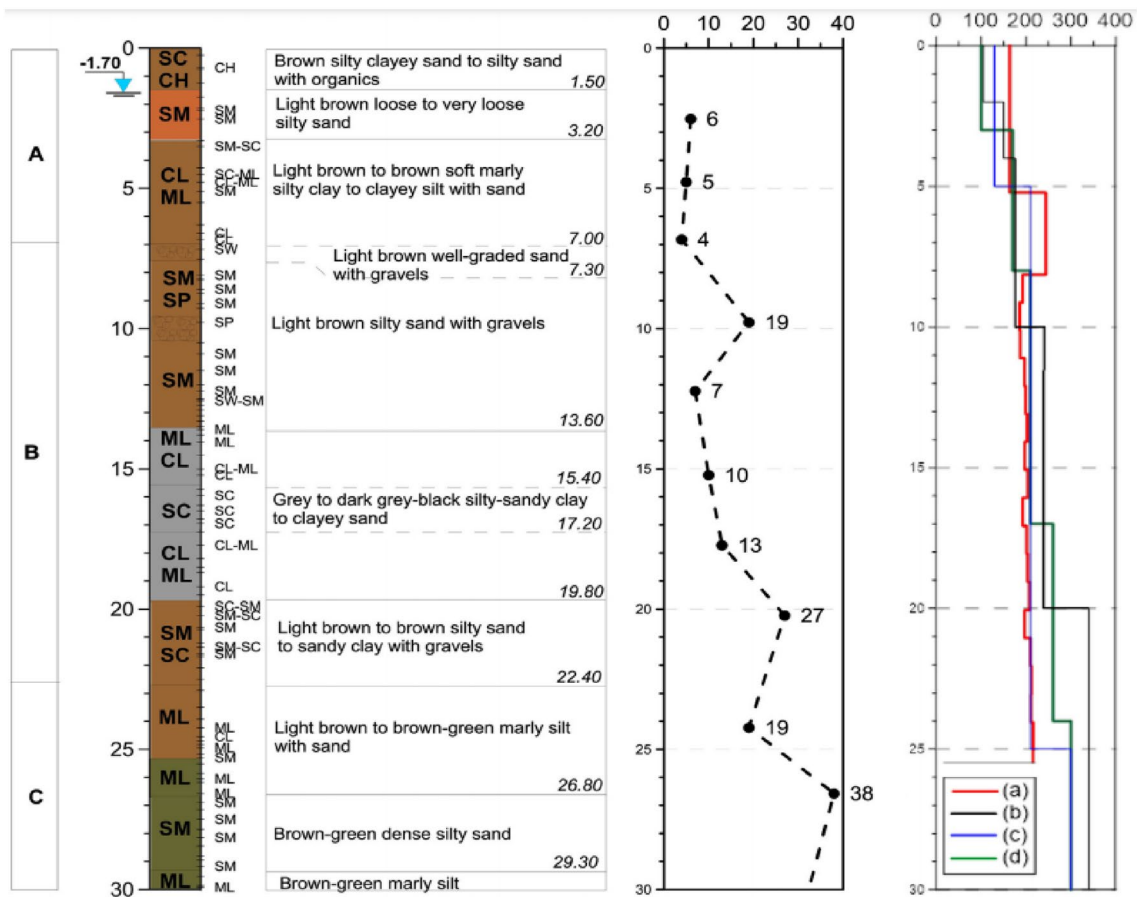


Fig. 2 Multi-span bridge with simply supported deck exposed to scour



**Fig. 3** Subsoil characteristics from the 30-m deep borehole BH-02 (left),  $N_{SPT}$  blow count from BH-02 (middle), and shear wave velocity profile in m/s (right) for cases **a** DH-01: DH test before EuroProteas' construction, **b**  $V_s$  values at a site approximately 50 m south of

EuroProteas [44], **c** reference model of the valley cross section from updated geophysical, geotechnical and numerical modelling [45], **d** profile from detailed geotechnical and geophysical surveys [46]. Adapted from Pitilakis et al. [6]

structure, which forms a 30° angle with the magnetic North. There is no particular criterion regarding the disposition. In theory, three accelerometers should be sufficient to describe the motion of the rigid base and top slabs. The consideration of the same location of the accelerometers at the top and the bottom was not feasible due to the presence of a shaker onto the top slab for the application of forced-vibration tests, which will be part of a future study. The recordings from these accelerometers mentioned above are later used to identify the dynamic response and the modal shapes of EuroProteas structure under various scour scenarios (see Sect. 4).

In addition to the prototype fully supported on the soil, two different scour scenarios were considered in the experimental campaign, corresponding to the scour widths  $S=0.3$  m and  $S=0.75$  m at the northern part of the foundation. Figure 5 depicts the excavated soil (i) during and (ii) at the end of the tests, after the superstructure was lifted. The considered scour hole shape can be assumed to be roughly representative of many scour holes that develop in real bridges with shallow rectangular foundation.

Lee et al. [26] have investigated this issue by performing a series of flume tests considering different typologies of foundations, as opposed to cylindrical monopiles, and found that the scour develops upstream of the pier, with the maximum scour depth attained at the nose of the footing. Alternative scour hole shapes could have been considered, but some preliminary numerical analyses considering different scour hole shapes for the same portion of eroded soil beneath the foundation had shown that this has a minor influence on the dynamic behaviour of the system. The effect of the scour hole shape is investigated numerically in Sect. 3.

### 3 Numerical modelling strategy

This subsection illustrates three three-dimensional numerical models developed to design the experimental full-scale tests and to predict the effects of scour on the foundation response and the variations of the soil–foundation–structure (SFS) system dynamic properties. In particular, various models were

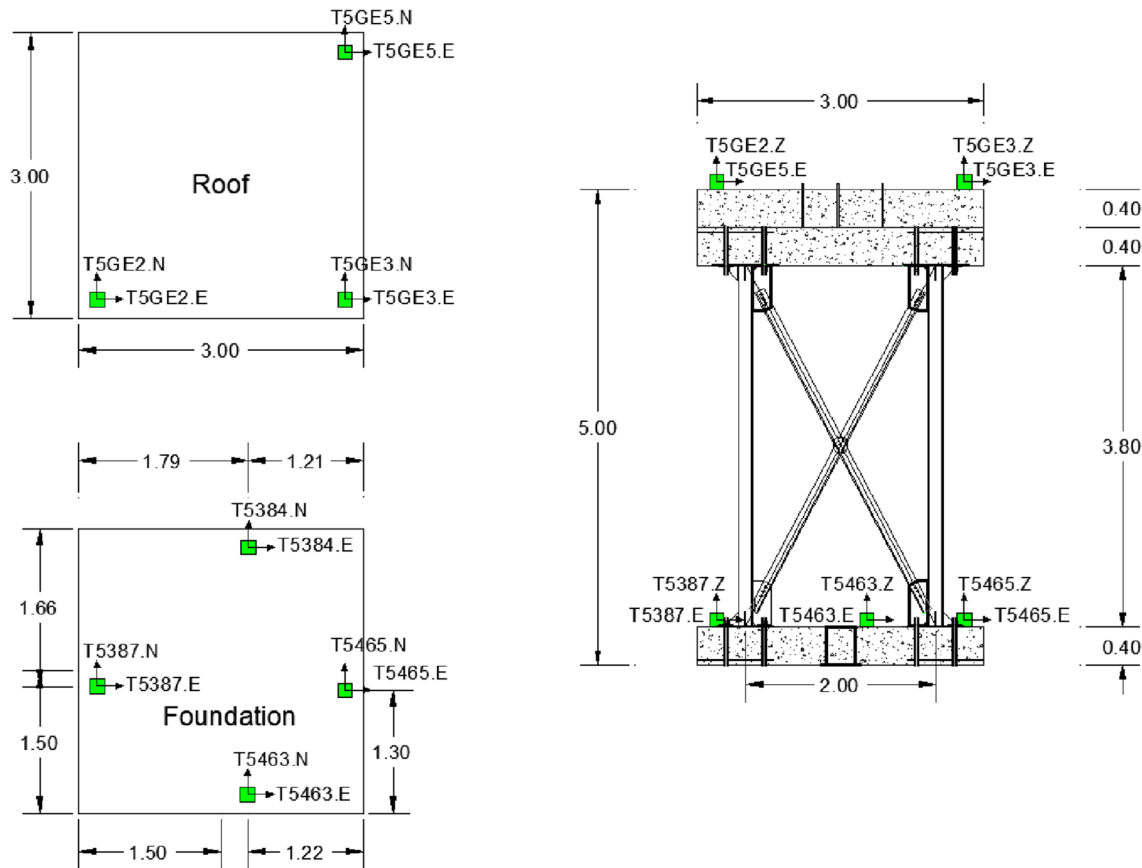


Fig. 4 Installed accelerometers on EuroProteas

**Table 1** Types and names of the installed accelerometers on EuroProteas

Accelerometers	
Type	Sensor
Güralp CMG-5T	T5463
Güralp CMG-5T	T5384
Güralp CMG-5T	T5465
Güralp CMG-5T	T5387
Güralp CMG-5TCDE	T5GE5
Güralp CMG-5TCDE	T5GE2
Güralp CMG-5TCDE	T5GE3

built in the Finite Element code Abaqus [47], namely, the Fixed Base (FB) structure, the structure with a continuous semi-infinite soil domain (SFS\_1), and the structure with the SFS modelled using linear springs and dashpots (SFS\_2), which simulate the impedance functions. A simplified version of the SFS\_2 model is also developed in Matlab [48], by employing a substructure approach and exploiting the impedance functions derived in a previous work by some of the authors [49] using a two-dimensional soil model (SFS\_3). The first two models developed in Abaqus share the same description of the superstructure (Fig. 6), with two-node linear



Fig. 5 i Excavation of the soil under the foundation, ii scour hole shape at the end of the final test

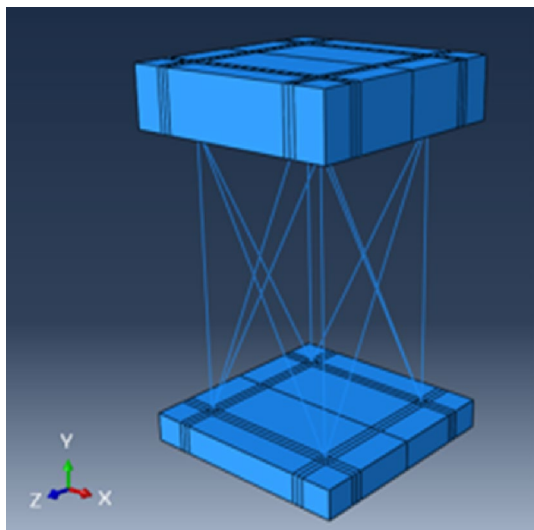


**Fig. 6** Superstructure used in fixed-base model

beam elements used to model the columns and the braces, and 20-node quadratic brick elements (C3D20) used to model the slabs. The columns are connected to the slabs using multi-point tie constraints, whereas the X-braces are connected to the column ends via a hinge connector. The connections between the two X-braces are based on joint connectors.

The steel Young's modulus and Poisson's ratio are  $E_s = 210,000$  MPa and  $\nu_s = 0.2$ , respectively, whereas the concrete mechanical properties are  $E_c = 29,962$  MPa and  $\nu_c = 0.2$ . A 1% damping factor is assigned to both materials using the following Rayleigh model. The Rayleigh damping coefficients are calibrated to achieve 1% damping factor in correspondence of the first and the third modes of vibration of the system, characterized by the highest participation of the superstructure masses along the  $x$  direction.

### 3.1 Fixed-base model (FB)

The FB model is obtained by restraining the displacements at the base of the foundation slab. This model, characterised by a fundamental vibration frequency of 9.26 Hz, is used to estimate the effects of Soil Structure Interaction (SSI) on the vibration properties by comparison with the other three designed models presented in the next subsections. The frequency of 9.26 Hz matches the ones evaluated in other studies on the same prototype [36].

### 3.2 Structure with soil modelled as a continuum with absorbing boundaries (SFS\_1)

This sub-section describes the three-dimensional model including the semi-infinite soil-domain. This domain is modelled with solid elements with elasto-plastic behaviour.

The elastic soil behaviour is described by assigning shear modulus  $G_s = 31.6$  MPa, soil density  $\rho = 1870$  kg/m<sup>3</sup>, shear wave velocity  $V_s = 130$  m/s and Poisson's ratio  $\nu = 0.3$ . The aforementioned values are consistent with the soil properties derived from BH-02 (Fig. 3) for the upper 5 m of the soil. It must be mentioned that the soil beneath EuroProteas mainly consists of sand, with the water level being 1.7 m under the ground surface. Therefore, for the sake of simplicity, a perfectly drained behavior has been assumed for the entire soil domain. Furthermore, the soil strength parameters are estimated from available laboratory and field SPT and CPT tests reported in [50]. More in detail, the plastic behaviour is defined by the Mohr–Coulomb model, with a friction angle  $\Phi = 30^\circ$ , and cohesion  $c' = 0.01$  MPa. The soil material damping is described through a 1% structural damping [47].

The interaction between the foundation and the soil is modelled using the “surface to surface” contact approach. The interface has a very high stiffness in compression to avoid penetration, can resist only compressive forces, and has a friction coefficient of  $\mu = 0.6$  along the tangential direction. The soil is represented by a finite domain with local Absorbing Boundary Conditions (ABCs) to avoid reflection of outgoing waves (Fig. 7). The length of the solid domain from the foundation slab outwards is 18 m; the absorbing elements are infinite brick elements, and their length is equal to that of the soil domain. To accurately model wave propagation, the mesh size satisfies the following relation [51]:

$$l_{\max} \leq \left( \frac{1}{8} \sim \frac{1}{5} \right) \lambda_{\min} \leq \frac{V_{s,\min}}{8f_{\max}} \quad (1)$$

where  $l_{\max}$  is the maximum element size,  $\lambda$  is shear wave-length, equal to 13 m,  $V_{s,\min}$  is the shear-wave velocity, equal

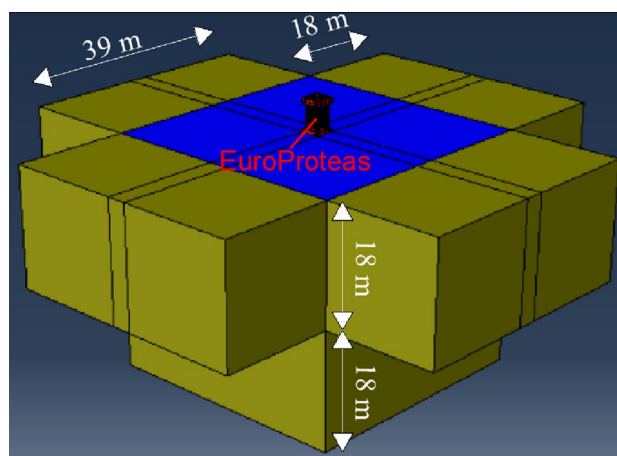


**Fig. 7** Model of SFS system with soil domain (in blue) and absorbing boundary conditions (in yellow) and the structure (in red) (color figure online)

to 130 m/s, and  $f_{\max} = 10$  Hz is the maximum frequency of interest.

In this model (denoted as “SFS\_1”), scour is characterised by a rectangular prism shape and it is simulated by removing soil elements under the foundation slab. To investigate how the scour hole shape affects the changes in fundamental frequency of the system, two variations of this model are developed. The first one (denoted as “SFS\_1\_TS”) considers a triangular prism shape of the scour hole, which extends not only beneath, but also beside the foundation and it is more representative of real scour conditions (see, e.g., [6] and [34]). The upstream scour slope is considered equal to  $\varphi = 30^\circ$ , while the downstream scour slope half of the upstream slope. It must be mentioned that since the soil domain is discretized using hexahedron elements, the scour slopes are simulated only approximately using a very refined mesh. The second model (denoted as “SFS\_1\_SS”) is developed by modifying the “surface to surface” contact interface between the soil and foundation, and removing the contact rather than soil elements beneath the foundation to simulate scour. In addition, the case of an embedded foundation is considered to represent not only more realistic conditions, where the foundation does not simply rest on the ground surface, but also an even more realistic scour hole shape based on the results of Lee et al. [26]. For this case, another two models are analysed, by removing not only the soil elements on the

upstream side of the foundation (i.e., the one perpendicular to the flow), but also on the other two sides of the foundation (i.e., the ones parallel to flow), for a width of 0.3 m. For this case two models are considered, namely, “SFS\_1\_RS\_E” and “SFS\_1\_TS\_E”, representing, respectively, a rectangular and a triangular scour hole shape. Figure 8 depicts the soil and contact conditions of the models with non-embedded foundations SFS\_1, SFS\_1\_TS and SFS\_1\_SS for a scour width of 750 mm, while Fig. 9 illustrates the geometry and the simulation of the scour hole for the models with embedded foundations SFS\_1\_RS\_E and SFS\_1\_TS\_E.

### 3.3 Structure with soil modelled using a simplified impedance function model (SFS\_2)

In this model, the semi-infinite soil-domain is replaced by a set of distributed springs and dampers with the aim of obtaining a simplified description of the SSI problem. This approach is similar to the one followed in Tubaldi et al. [6] and Scozzese et al. [34], with zero-thickness cohesive interface elements resisting only compression stresses at the bottom of the foundation describing the soil reaction. The cohesive interface elements have a visco-elastic behaviour in compression, with properties based on the work of Gazetas [52]. The springs constants (stresses per unit displacements) have been evaluated as follows:

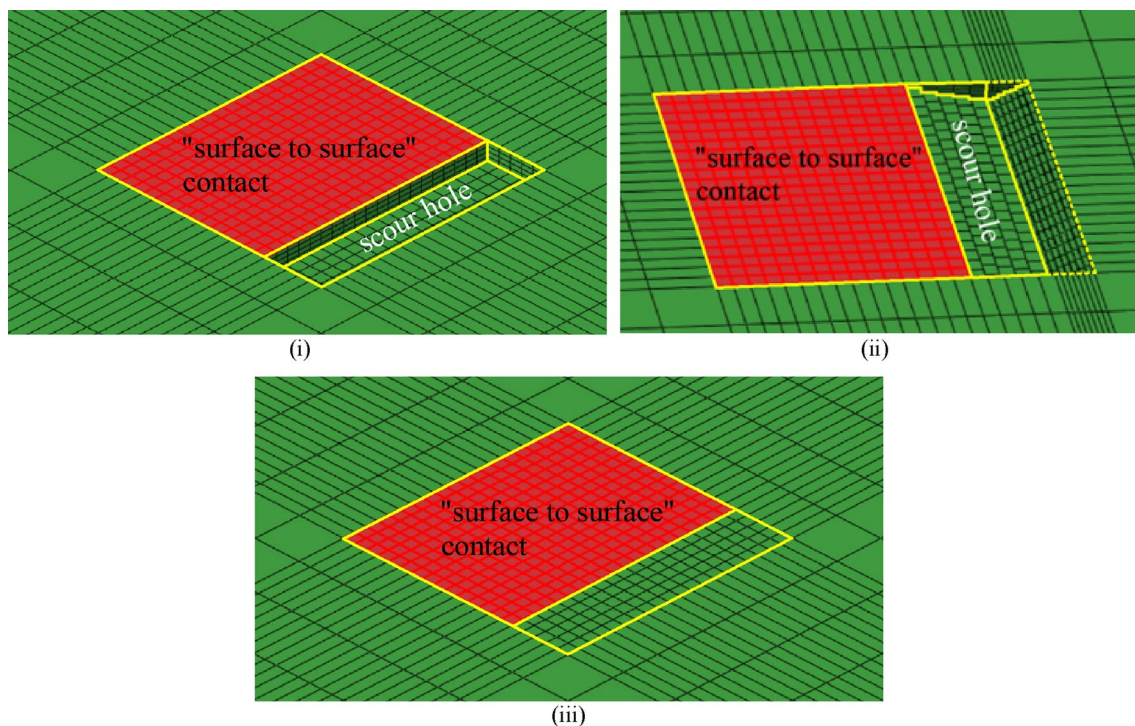


**Fig. 8** Simulation of scour hole at the soil domain of the model **i** SFS\_1, **ii** SFS\_1\_TS, and **iii** SFS\_1\_SS



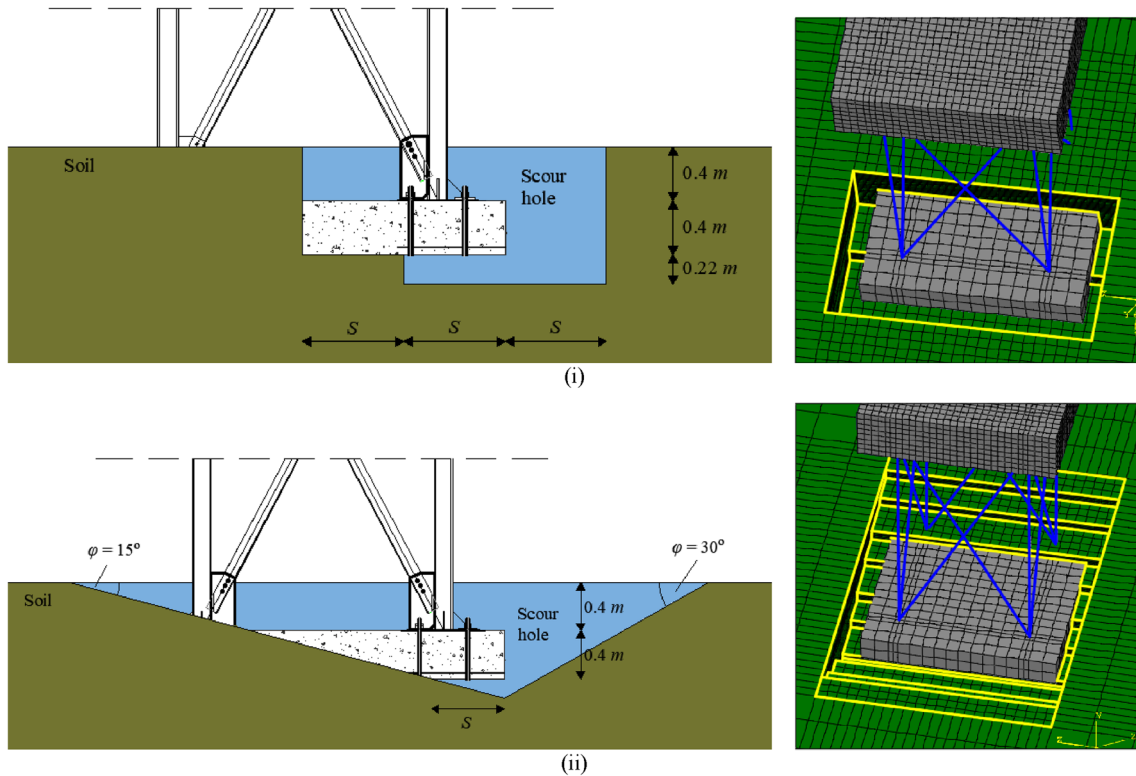


Fig. 9 Geometry and simulation of the scour hole around the embedded foundation for the model i SFS\_1\_RS\_E and ii SFS\_1\_TS\_E

$$k'_{s,x} = \frac{k_{s,x}}{A_x} \quad k'_{s,y} = \frac{k_{s,y}}{A_y} \quad k'_{s,z} = \frac{k_{s,z}}{A_z}, \tag{2}$$

where  $k_{s,x}$ ,  $k_{s,y}$  and  $k_{s,z}$  are given by Gazetas [52] as a function of the shear modulus,  $G_s = V_s^2 \rho = 31.6$  MPa, the Poisson's ratio,  $\nu = 0.3$ , and of the foundation geometry, whereas  $A$  is the foundation area in contact with the soil.

The dashpots are in parallel with the springs and represent the soil radiation damping according to the following expression [52]:

$$\begin{aligned} c'_x &\simeq (\rho V_s) \cdot \tilde{c}_x, \quad c'_z \simeq (\rho V_s) \cdot \tilde{c}_z \\ c'_y &\simeq (\rho V_{La}) \cdot \tilde{c}_y \end{aligned} \tag{3}$$

where  $\rho$  is soil material density,  $V_{La}$  is Lysmer's shear wave velocity, related to  $V_s$ , and  $\tilde{c}_x$ ,  $\tilde{c}_y$  and  $\tilde{c}_z$  are function of the foundation geometry and mechanical soil properties. A 5% hysteretic damping factor is also considered to describe the energy dissipation within the soil domain. In this work, it is assumed that the springs and the dashpots are frequency independent, and the values of  $k_{s,x}$ ,  $k_{s,y}$ ,  $k_{s,z}$  and of  $\tilde{c}_x$ ,  $\tilde{c}_y$ ,  $\tilde{c}_z$  are those corresponding to the system natural frequency. A more sophisticated model could consider the variation with frequency of these parameters. The values of the subgrade reactions are  $k'_{s,x} = 27.9 \times 10^6$  N/m<sup>3</sup>,  $k'_{s,z} = 27.9 \times 10^6$  N/

m<sup>3</sup>, and  $k'_{s,y} = 34.2 \times 10^6$  N/m<sup>3</sup>. The values of the damping coefficients (including the hysteretic component) are  $c'_x = 33.83 \times 10^5$  N s/m,  $c'_z = 30.44 \times 10^5$  N s/m, and  $c'_y = 30.44 \times 10^5$  N s/m.

To simulate scour in Abaqus [47], the “model change” capability is employed, allowing to progressively eliminate the cohesive interface elements at the foundation–soil interface that represent the portion of eroded soil.

### 3.4 Two-dimensional structure and soil model (SFS\_3)

A three-dimensional model with absorbing boundaries conditions is expected to provide a more accurate description of the behavior of the system. However, it is computationally demanding. In this subsection, a simplified but robust numerical approach is employed for investigating the influence of scour on the dynamic response of systems with shallow foundation, which is based on two-dimensional description of the problem. This approach can be employed for a preliminary assessment of the effects of scour in terms of change of modal properties. The approach is based on the work of Antonopoulos et al. [49], where the influence of scour on the dynamic response of SFS systems was investigated by applying the substructure method [53]. In particular, non-dimensional

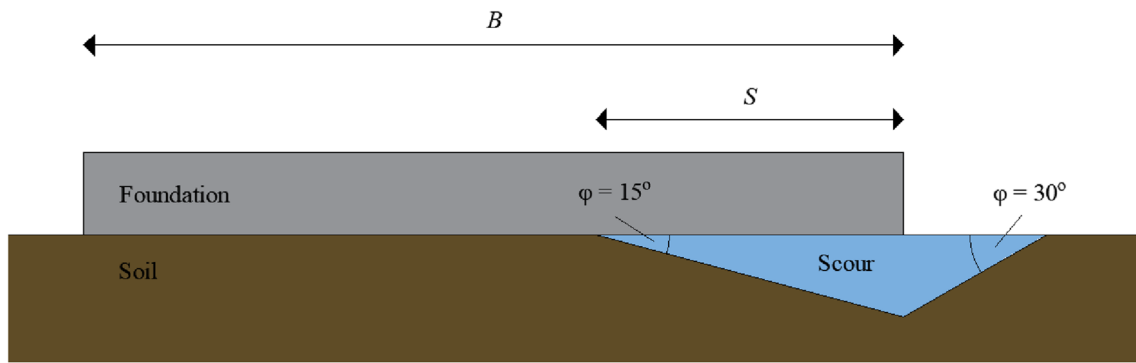


Fig. 10 Shape of the triangular scour holes considered within the two-dimensional modelling approach

frequency dependent impedance functions were obtained for a rigid strip foundation resting on an homogenous elastic soil domain for the case of no scour and for various scour hole shapes. The numerical model used to derive the impedance function was developed in Abaqus [47] using a plain-strain assumption, and it was validated based on the comparison between the impedance functions obtained numerically and the ones reported in Hryniewicz [54]. Figure 10 illustrates the shape of the scour hole considered in Antonopoulos et al. [49]. The derived impedance functions were used to evaluate the reduction of the fundamental vibration frequency of vibration of a simple SFS system (Fig. 11) for increasing levels of scour. The same approach is adopted here to evaluate the effects of scour on the Europroteas' prototype.

The simplified model of EuroProteas consists of a superstructure with lumped mass  $m_s = 18.32$  Mg, height  $h_s = 4.2$  m, and lateral stiffness  $k_s = 62,016.49$  kN/m, based on a shallow foundation of mass  $m_f = 9.16$  Mg, height  $2h_f = 0.4$  m, width  $2b_f = 3$  m and mass moment of inertia  $I_f = 6.99$  Mg m<sup>2</sup>. The compliance of the soil-foundation system is described by means of the impedance functions  $\bar{k}_{xx}$  for the horizontal response,  $\bar{k}_{r,y,r,y}$  for the rotational response, and  $\bar{k}_{x,r,y}$  for the coupled roto-translational response of the foundation, which can be taken directly from Antonopoulos et al. [49], where they are reported in non-dimensional form. Obviously, different impedances have to be considered for each investigated scour scenario.

The free vibration equation of motion of the SFS system can be expressed in the frequency domain in a vector form as:

$$-\omega^2 \mathbf{M}\bar{\mathbf{U}} + i\omega \mathbf{C}(\omega)\bar{\mathbf{U}} + \mathbf{K}(\omega)\bar{\mathbf{U}} = 0 \tag{4}$$

where  $\bar{\mathbf{U}}$  denotes the Fourier transform of the vector  $\mathbf{U}$  collecting the three generalised displacements of the system in the time domain, namely, the foundation translation ( $u_f$ ) and rotation ( $\theta_f$ ), and the relative displacement ( $u_s$ ) of mass  $m_s$  with respect to the base (see Fig. 11). Furthermore,  $\mathbf{M}$ ,  $\mathbf{C}$  and  $\mathbf{K}$  are the mass, damping and stiffness matrices of the system. These quantities are expressed as follows [55]:

$$\mathbf{U} = [u_f \quad \theta_f \quad u_s]^T \tag{5}$$

$$\mathbf{M} = \begin{bmatrix} m_f + m_s & m_f h_f + m_s h & m_s \\ m_f h_f + m_s h & I_f + m_f h_f^2 + m_s h^2 & m_s h \\ m_s & m_s h & m_s \end{bmatrix} \tag{6}$$

$$\mathbf{C}(\omega) = \begin{bmatrix} c_{xx}(\omega) & b_f c_{x,r,y}(\omega) & 0 \\ b_f c_{x,r,y}(\omega) & b_f^2 c_{r,y,r,y}(\omega) & 0 \\ 0 & 0 & c_s \end{bmatrix} \tag{7}$$

$$\mathbf{K}(\omega) = \begin{bmatrix} k_{xx}(\omega) & b_f k_{x,r,y}(\omega) & 0 \\ b_f k_{x,r,y}(\omega) & b_f^2 k_{r,y,r,y}(\omega) & 0 \\ 0 & 0 & k_s \end{bmatrix} \tag{8}$$

Equation (4) is solved repeatedly, considering each time the values of  $\bar{k}_{xx}$ ,  $\bar{k}_{x,r,y}$ ,  $\bar{k}_{r,y,r,y}$  that correspond to an excitation frequency  $\omega$ . Each solution provides a value of the natural frequency  $\tilde{\omega}$ , and the correct one satisfies the equation  $\omega = \tilde{\omega}$ .

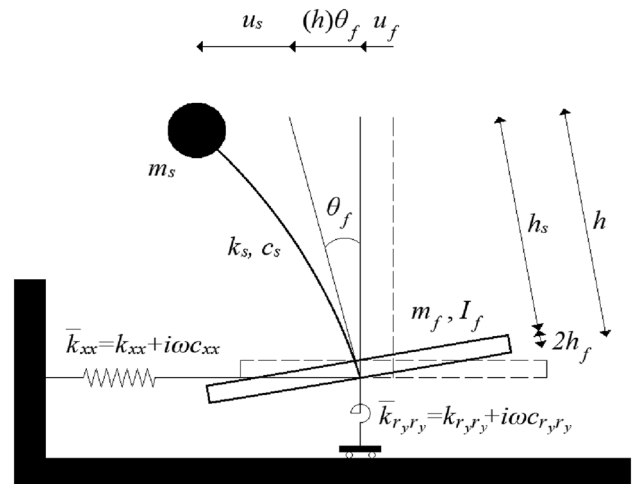


Fig. 11 Model of the SFS\_3 system (coupling terms are not illustrated)

### 3.5 Eigenvalue analyses and validation of the modelling strategies

A preliminary validation of the developed modelling strategies was carried out before undertaking the experiments, based on the comparison of the eigenvalue analysis results with the experimental model properties obtained by an earlier experimental campaign [36] for the case of no scour. The experimental results were obtained by Pitilakis et al. [36] by recording ambient vibration signals by means of accelerometers located on the EuroProteas and applying the Frequency Domain Decomposition (FDD) method. Table 2 shows the estimated resonance frequencies of EuroProteas for each numerical model. These frequencies refer to the vibration in the horizontal direction. It can be noted that the resonant frequency of the system reduces significantly if soil–structure interaction effects are taken into account, and that there is a good agreement between the estimates of the frequency provided by the various models and the experimental one. Evaluating the modal frequencies of interest in Abaqus [47] is challenging, due to the presence of many modes involving only the 3D soil domain and not the superstructure, and the uncertainty in the contribution of the infinite elements at the boundaries. For this reason, the vibration frequency obtained from modal analysis of the model SFS\_1 has been checked against that evaluated from free-vibration analysis.

### 4 Free-field tests results and comparison with the numerical studies

Ambient vibrations signals were recorded by the accelerometers before inducing scour and for two different stages of scour, corresponding to the scour widths of  $S=0.3$  m and  $S=0.75$  m (see Fig. 10 for definition of  $S$ ). The identification of the modal parameters of the SFS is carried out using the Frequency Domain Decomposition (FDD) method proposed by Brincker et al. [56].

Figure 12 illustrates the singular value of the power spectral density matrix of the response of the SSI system to the ambient vibration before inducing scour. It can be observed that the system response at the various frequencies is dominated by the first singular value, and that the peaks corresponding to the first three modes are visible. These three vibration modes are illustrated in Fig. 13 together with the corresponding modal vibration frequencies.

The first two vibration modes correspond to the vibration of the system along two orthogonal directions that are rotated with respect to the principal axes of the superstructure (Fig. 13). The third mode is associated with the torsion of the superstructure about the vertical axis. This may be due to a non-perfect contact between the base of the structure and the soil. Particularly, Fig. 5ii illustrates the soil beneath

**Table 2** Fundamental frequency of vibration for different structural configurations (case without scour)

Structural configuration	Frequency (Hz)	
	Abaqus	Experimental
FB model	9.26	–
SFS_1 model	4.73	4.1
SFS_1 model (Free vibration)	4.73	
SFS_2 model	4.42	
SFS_3 model	4.64	

the foundation after the removal of the structural prototype at the end of the experimental campaign. It can be observed that vegetation was found both in the area of the scour hole, and the southwest part of the foundation. This suggests that there was possibly a non-perfect contact between the soil and the foundation, resulting in water ingress and growth of vegetation where this contact was missing. This asymmetry in the foundation support could explain the differences between the simulated dynamic behaviour and the experimental one. This issue is discussed in detail in Sect. 5. Furthermore, this might explain the fact that the frequencies of the experimental first two modes of vibration (i.e., 3.51 Hz and 4.5 Hz) are, respectively, higher and lower than the value of 4.1 Hz reported in [36]. This value was obtained in a previous experimental campaign on the same prototype and could be representative of the first two modes of vibrations, assuming that there was a perfect contact between the foundation and the soil.

It is noteworthy that for the purpose of performing the tests, the prototype was moved in another location, 20 m apart from the one of [36]. Thus, the differences in the frequency may also be explained by slight variations in the soil properties from one location to the other. The “x” symbols on the plan views of Fig. 13 indicate the location of the accelerometers (Table 1) installed on the roof and foundation slab of EuroProteas.

Figure 14 illustrates the variation of the modal frequencies with the scour width normalized by the foundation width ( $S/B$ ). It can be observed that all these frequencies vary linearly with  $S/B$ . The frequency of the first mode is more sensitive to scour, as expected due to the location of the scour hole. In the same figure, the vibration frequencies of the numerical models SFS\_1, SFS\_2 and SFS\_3 are plotted. It is worth to note that results from the numerical models are not in a great agreement with those from the experimental tests. In particular, the numerical models overestimate the first vibration frequency for all the investigated  $S/B$  values, whereas they underestimate the effects of scour in terms of frequency reduction in the case of the second mode. Moreover, it is noteworthy that the numerical models are characterized by two identical translation modes

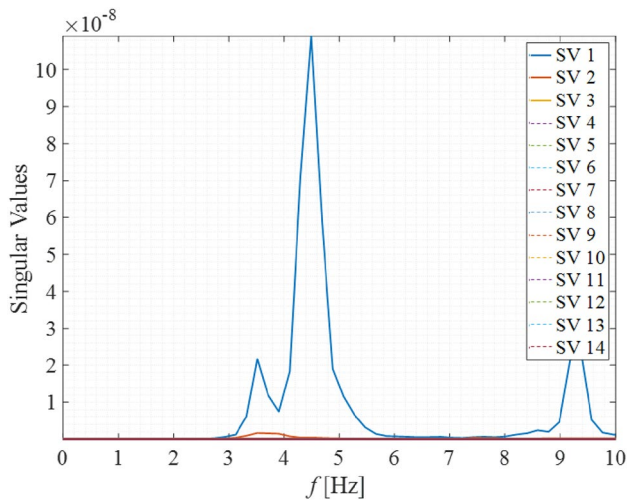


**Fig. 12** Singular values (SVs) of the PSD matrix of the response to ambient vibration in the case of no scour

in the  $x$  and  $y$  directions in the case of no-scour whereas the experimental modes are different and coupled in the translational directions due to possible asymmetries in the foundation–soil contact area. It is also observed that the SFS\_2 model cannot capture satisfactory the frequency of the rotational mode shape, contrary to the SFS\_1 model. The reasons for the difference between the experimental and numerical results and the updating of the model to better capture the observed modal properties are discussed in detail in the next sections.

The effect of the scour hole shape on the dynamic behaviour of EuroProteas is investigated by comparing the results obtained with the models SFS\_1, SFS\_1\_TS and SFS\_1\_SS, described in Sect. 3. Figure 15 shows the variation of the vibration frequencies vs the normalised scour width  $S/B$  for the various numerical models. The scour hole shape has only a minor effect on the variation of frequency of the system, which is mainly controlled by the normalised scour width. The triangular prism shape, which is more representative of real scour conditions, yields slightly higher frequencies than the rectangular one. Similarly, the case of SFS\_1\_SS, which simulates scour only by removing the contact between the foundation and soil rather than the soil elements under the foundation, yields results similar to the triangular prism shape.

Further analyses are made considering the case of embedded foundation. Table 3 compares the vibration frequencies obtained for the models SFS\_1, SFS\_1\_TS, SFS\_1\_RS\_E and SFS\_1\_TS\_E. It can be observed that the models with embedded foundation exhibit higher vibration frequencies compared to the models with the shallow foundation. In addition, for the embedded foundation, the shape of the scour hole was found to have a negligible influence on the vibration frequencies.

Figure 16 compares the normalised vibration frequencies  $f_{\text{scour}}/f_{\text{no,scour}}$  for increasing normalised scour width  $S/B$  for the various models analysed. Similar to the models with surface foundations, the models with embedded foundation exhibit a linear reduction of the vibration frequencies for increasing scour width. However, the models with embedded

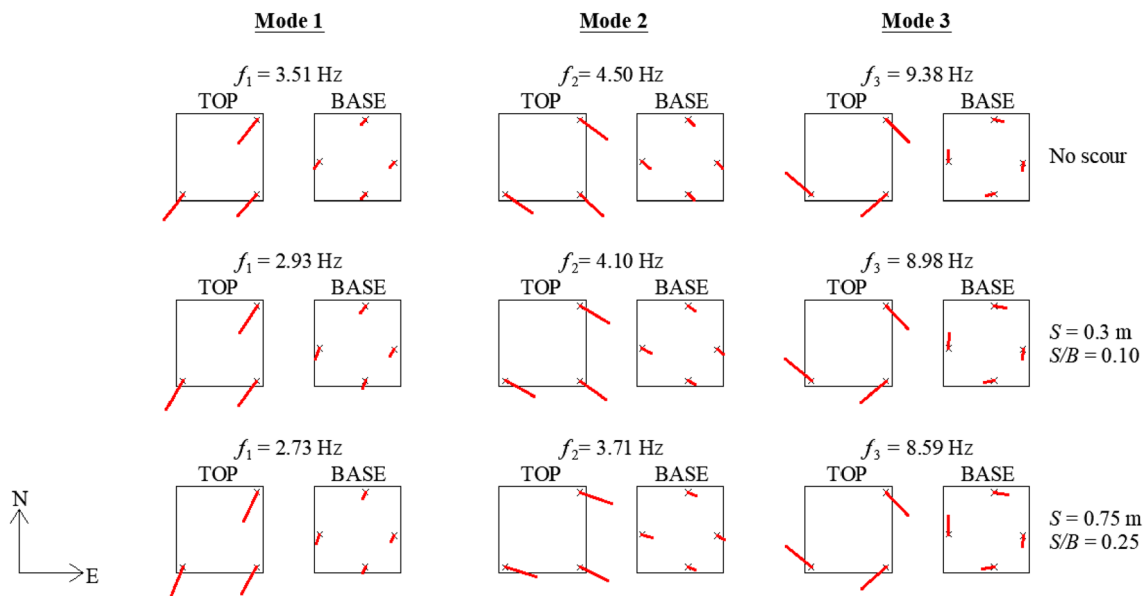


**Fig. 13** Experimental modal shapes for system with no scour, and normalised scour widths  $S/B=0.1$  m and  $S/B=0.25$  m. Plan view of top and base horizontal displacements

foundation are slightly more sensitive to scour than the models with surface foundation, i.e., for the same value of the normalised scour width, slightly higher frequency reductions are observed. This is because for a given value of  $S/B$ , larger portions of soil, contributing to the stiffness of the system, are removed. For the sake of completeness, Table 4 shows the reduction of the vibration frequencies of the models SFS\_1, SFS\_1\_TS, SFS\_1\_RS\_E and SFS\_1\_TS\_E for increasing scour widths with respect to the case of no scour.

The stress distribution of the soil in the vicinity of the scour hole is also investigated considering model SFS\_1 to provide a more complete description of the effects of scour. Specifically, Fig. 17 illustrates the vertical stresses in the soil surrounding the foundation for two different scour scenarios ( $S/B=0$  and  $S/B=0.25$ ). As it can be observed, scour affects the stress distribution at the soil beneath the foundation, which becomes not uniform, with high stresses localised under the foundation close to the scour hole. This is expected, due to the eccentricity between the resultant of the loads transmitted from the superstructure and the centre

of the area of the foundation–soil interface providing a reaction. Nevertheless, these stresses are not expected to induce significant inelastic strains in a large portion of soil.

In general, scour is expected to affect differently the vibration frequencies of different bridge typologies. To investigate this issue, some comparisons are made with the results obtained numerically in a previous study by some of the authors of this paper on Rubbianello bridge [34]. This is a multi-span masonry arch bridge with shallow foundations, which partially collapsed due to scour. Figure 18 compares the variation of the  $f_{scour}/f_{no\ scour}$  ratio with the normalised scour width ratio  $S/B$  obtained for EuroProteas (SFS\_1) and for the Rubbianello bridge. It must be mentioned that in case of Rubbianello bridge only one pier is subjected to scour, and that the shallow foundation is embedded below the ground. Thus, the case of no scour (i.e.,  $S/B=0$ ) corresponds to a scour depth equal the embedded depth of the foundation. It can be observed that in both the cases the reduction of frequency with the increase of the normalized scour width is linear.

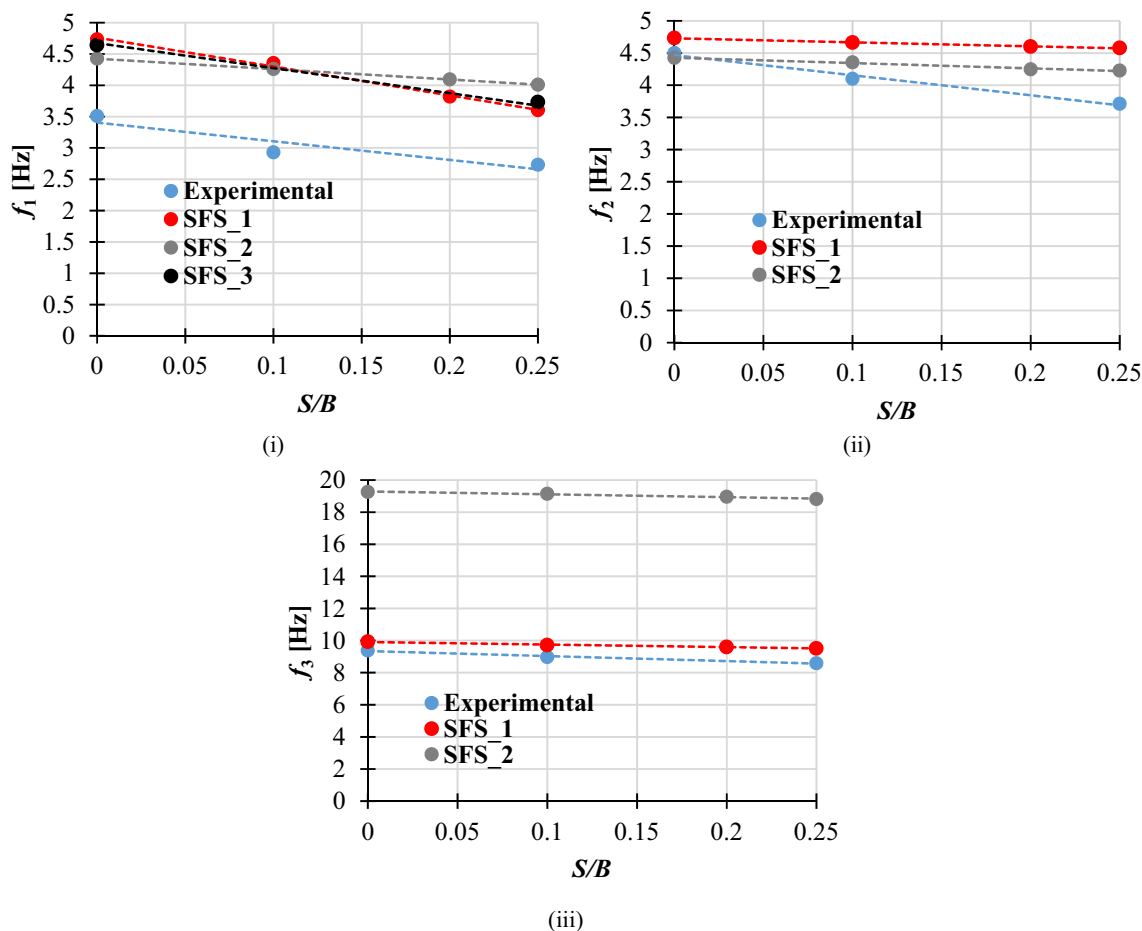


Fig. 14 Variation of the vibration frequencies of the i) first, ii) second and iii) third monitored mode with the normalized scour width  $S/B$  according to experimental and numerical results from the models SFS\_1, SFS\_2 and SFS\_3

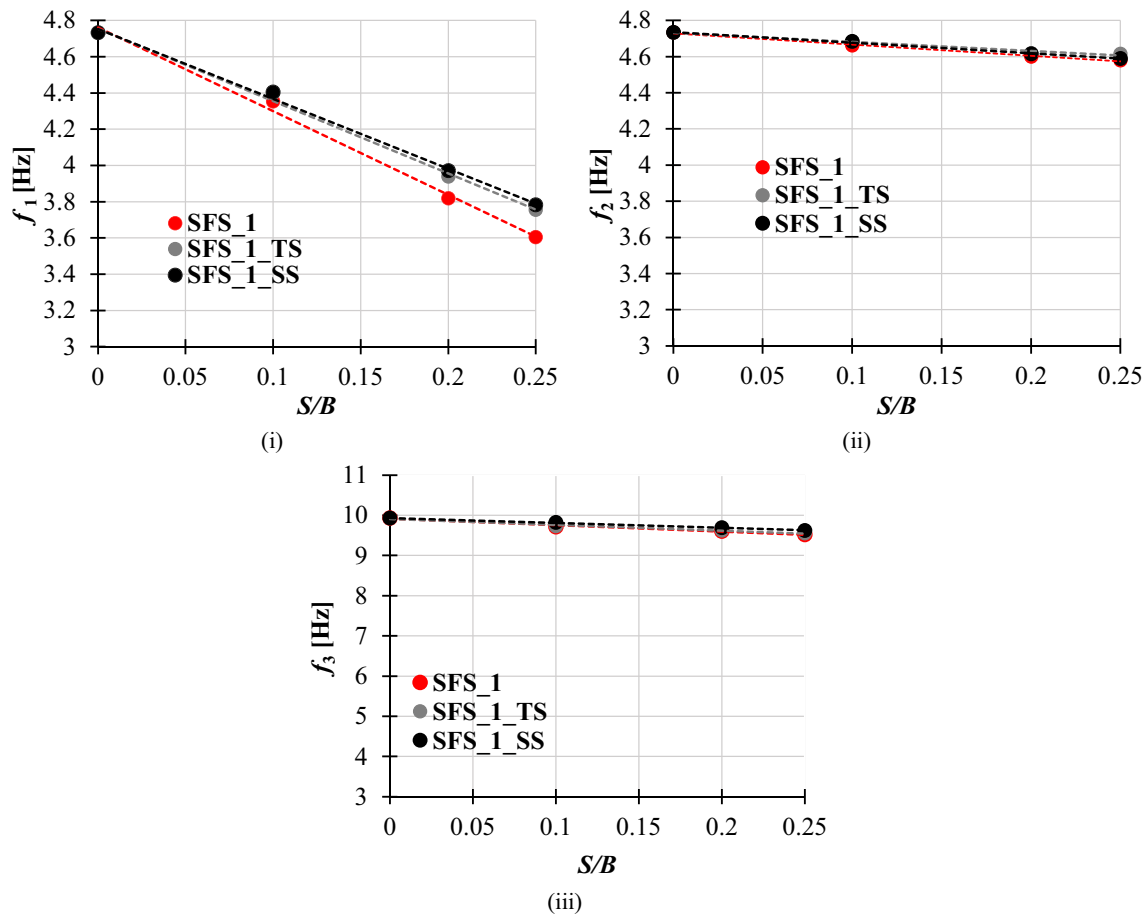


Fig. 15 Comparison of monitored modes between the models SFS\_1, SFS\_1\_TS and SFS\_1\_SS

However, in the case of the masonry arch bridge model, the rate of decay of the frequency is higher. This can be explained by the fact that the superstructure of Europroteas undergoes an almost rigid movement and remains linear elastic even for large scour widths, whereas the masonry arch bridge undergoes severe damage and cracking. Thus, the change of frequency reflects not only the change of boundary conditions and reduction of support, but also the degradation of the system (i.e., reduction of tangent stiffness). To have more insight into how scour affects the changes of frequency in the case of different soil, foundation

and superstructure properties, reference can be made to the results of the parametric study reported in [49].

### 5 Model updating

This subsection describes the updating of the numerical model SFS\_1 carried out to obtain a better agreement with the experimental results. As discussed in Sect. 4, the presence of vegetation in the area of scour hole and under the southwest part of the foundation of EuroProteas suggests a

Table 3 Fundamental vibration frequencies of the models SFS\_1, SFS\_1\_TS, SFS\_1\_RS\_E and SFS\_1\_TS\_E for increasing scour width

Models	$f_1$ (Hz)				$f_2$ (Hz)				$f_3$ (Hz)			
	$S/B$				$S/B$				$S/B$			
	0	0.1	0.2	0.25	0	0.1	0.2	0.25	0	0.1	0.2	0.25
SFS_1	4.73	4.35	3.382	3.60	4.73	4.66	4.60	4.58	9.93	9.72	9.61	9.50
SFS_1_TS	4.73	4.44	3.94	3.75	4.73	4.68	4.62	4.59	9.93	9.73	9.62	9.55
SFS_1_RS_E	5.39	4.91	4.46	4.13	5.39	5.24	5.08	4.95	10.17	10.02	9.94	9.89
SFS_1_TS_E	5.39	4.89	4.45	4.08	5.39	5.12	4.95	4.87	10.17	10.02	9.96	9.90

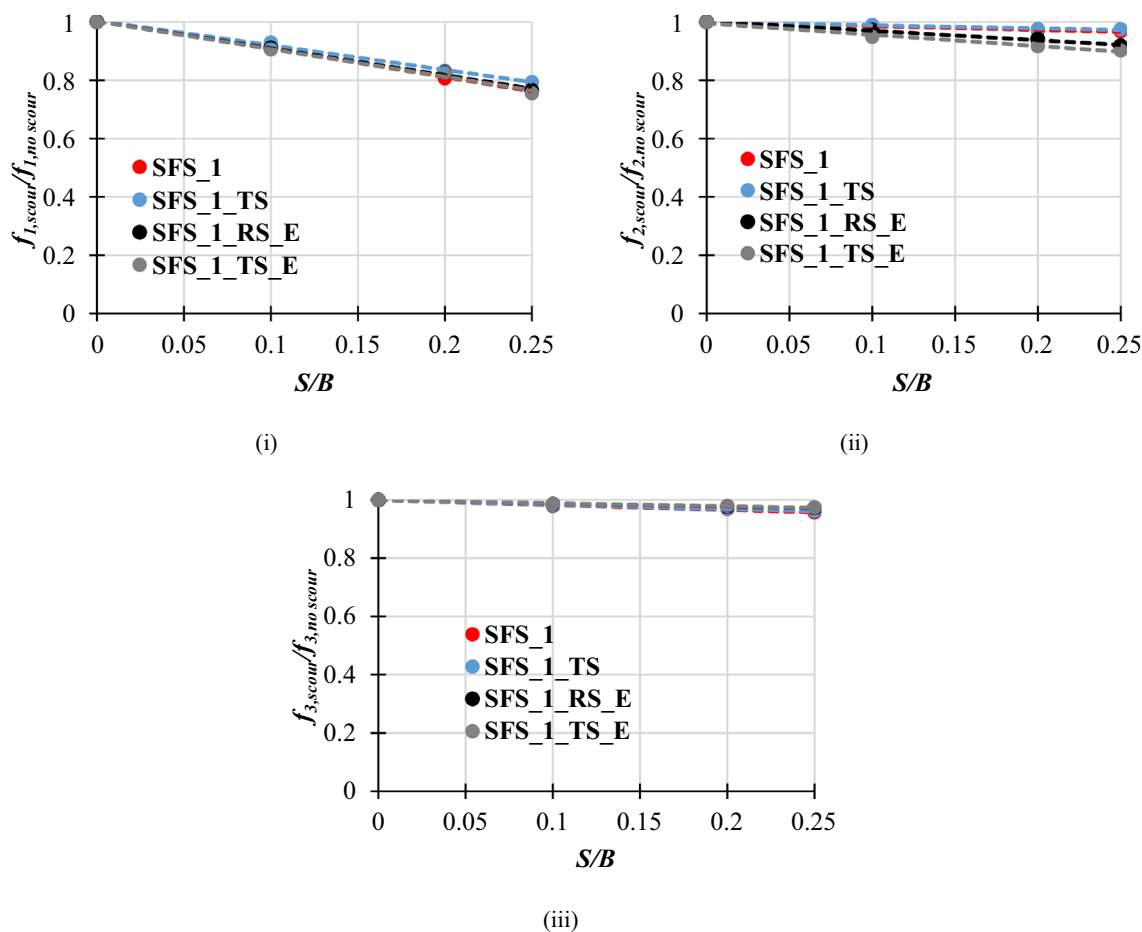


**Fig. 16** Comparison of the normalised vibration frequencies for increasing scour width between the models SFS\_1, SFS\_1\_TS, SFS\_1\_RS\_E and SFS\_1\_TS\_E

non-perfect contact between the soil and foundation. This explains the discrepancy in the dynamic behaviour of Euro-Proteas between the experiments and the numerical models based on a perfect soil–foundation contact. To study this issue, the model SFS\_1 is considered in this section and updated to better simulate the obtained experimental results. Models SFS\_2 and SFS\_3 are not herein considered, although they are computationally more efficient than model SFS\_1, because they cannot fully describe the dynamic behaviour of the system.

To simulate the lack of full support of the foundation at the beginning of the test, the soil elements of model SFS\_1 are removed under the foundation at the location where vegetation was found (Fig. 5ii) and modal analysis is run again on the updated model. Figure 19 illustrates the contact area between the soil and foundation for each of the examined scour scenarios.

The results of the modal analyses of the updated model are presented below and the consistency between the experimental and numerical results is investigated by both

**Table 4** Reduction of the vibration frequencies for increasing scour widths with respect to the case of no scour

Models	Reduction of $f_1$ (%)			Reduction of $f_2$ (%)			Reduction of $f_3$ (%)		
	$S/B$			$S/B$			$S/B$		
	0.1	0.2	0.25	0.1	0.2	0.25	0.1	0.2	0.25
SFS_1	8.01	19.33	23.86	1.49	2.81	3.25	2.16	3.21	4.33
SFS_1_TS	7.07	16.79	20.66	1.04	2.43	2.48	2.01	3.12	3.82
SFS_1_RS_E	8.97	17.39	23.49	2.78	5.88	8.20	1.50	2.28	2.73
SFS_1_TS_E	9.41	17.40	24.44	5.11	8.31	9.80	1.48	2.11	2.66

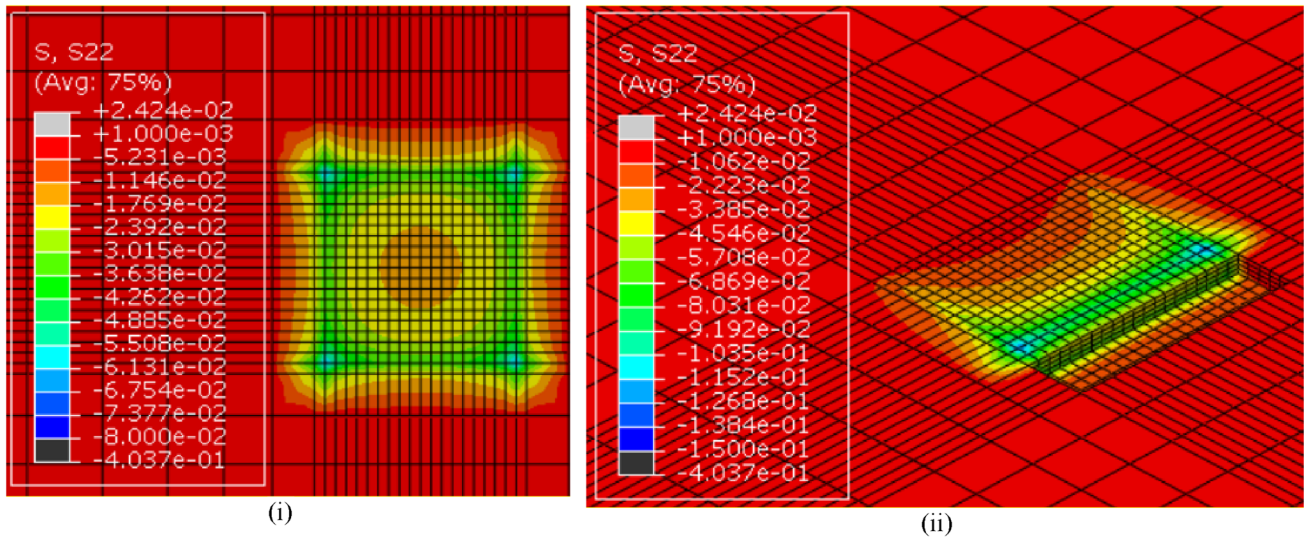


Fig. 17 Vertical stresses distribution of the soil of the model SFS\_1 for i  $S/B=0$  and ii  $S/B=0.25$  (unit of MPa)

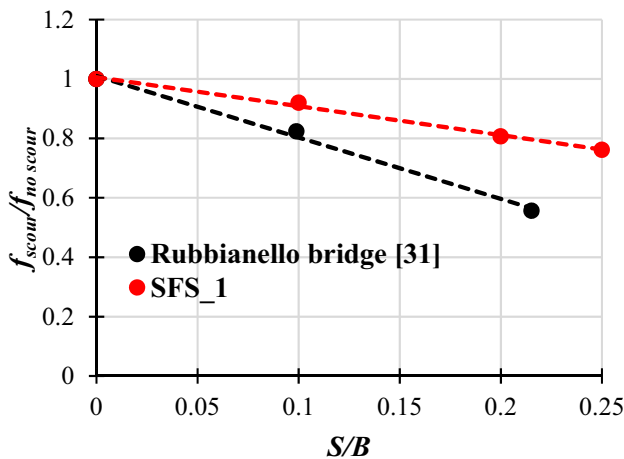


Fig. 18 Comparison of the non-dimensional ratio  $f_{scour}/f_{no\_scour}$  between EuroProteas and Rubbianello bridge

comparing resonance frequencies and mode shapes. As for the latter, the Modal Assurance Criterion (MAC) [57] is used to evaluate the matching of numerical and experimental mode shapes.

Figure 20 illustrates the corresponding modal shapes and vibration frequencies of EuroProteas. It can be noticed that the modal shapes are now in a very good agreement with the experimental ones, and the coupling is observed between the responses in the N–S and E–W directions.

The Modal Assurance Criterion (MAC) is a useful tool for comparing pairs of modal shapes derived from numerical models to those obtained experimentally. In more detail, it is a statistical indicator sensitive to small differences in the modal shapes with values between 0 and 1, indicating null

or absolute consistency between the compared pairs of mode shapes, respectively, while values higher than 0.8 indicate a satisfactory consistency. It must be mentioned that MAC must not be used for validation of the mode shapes, but solely for investigating the consistency. This is due to the fact that (i) it is unable to identify if the modal vectors are orthogonal or incomplete and (ii) it is unable to distinguish systematic errors from local discrepancies [57]. For this reason, it is important that the modal shapes to be matched are identified before applying the MAC.

Equation (9) expresses the MAC for two sets of mode vectors,  $\varphi_r$  and  $\varphi_q$ :

$$MAC(r, q) = \frac{|\varphi_r^T \varphi_q|^2}{(\varphi_r^T \varphi_r)(\varphi_q^T \varphi_q)} \tag{9}$$

where the symbol T denotes the transpose.

Table 5 shows the values of MAC between the experimental and numerical modes. A satisfactory consistency is achieved for all the modes and scour conditions investigated, with values significantly higher than 0.8. The torsional modal shape in particular is very well captured by the updated numerical model, whose performance generally improves for increasing levels of scour.

Figure 21 illustrates the variation of the vibration frequencies of the updated system for increasing scour widths, together with the experimental ones. It can be noted that by updating the model SFS\_1, there is also very good agreement in regards to the frequency variation. These results suggest that the assumption of a non-perfect contact between foundation and soil is valid and can explain the observed experimental results.



## 6 Conclusions

This paper has presented the results of an experimental campaign and numerical simulation aimed at evaluating the influence of scour on the dynamic behaviour of a structural prototype with shallow foundation. To the authors' best knowledge, this is the first study that investigates this through a full scale free-field experiment. The experimental testing campaign have also been complemented by extensive numerical analyses, investigating different modelling approaches for simulating the effects of scour on structural systems with shallow foundations.

The following observations can be made regarding the ambient vibration test results:

- a significant coupling was observed in the translational modes of vibration, even though the superstructure of EuroProteas is a symmetric system along both the horizontal principle axes. This was explained by the established non-uniform contact between the foundation and the soil. Although this result cannot be generalised and

is out of interest, it is indeed very important and demonstrates the impact of the various uncertainties and not controllable/unexpected factors that accompany in-field testing.

- a linear reduction of the vibration frequencies of the three modes investigated (two translational plus one torsional) is observed for increasing scour widths. The reduction of frequency of vibration for 1/4 of scoured foundation width is of the order of 30%, 18% and 8%, respectively, for the first, second and third vibration mode.

Based on the simulation of the experimental tests, the following conclusions can be drawn:

- the investigated modelling approaches provide similar results in terms of reduction of vibration frequency of the system for increasing scour widths;
- the vibration frequencies of the system reduce significantly for increasing values of the normalised scour width, whereas they are not significantly affected by the scour hole shape (e.g., rectangular or triangular); the

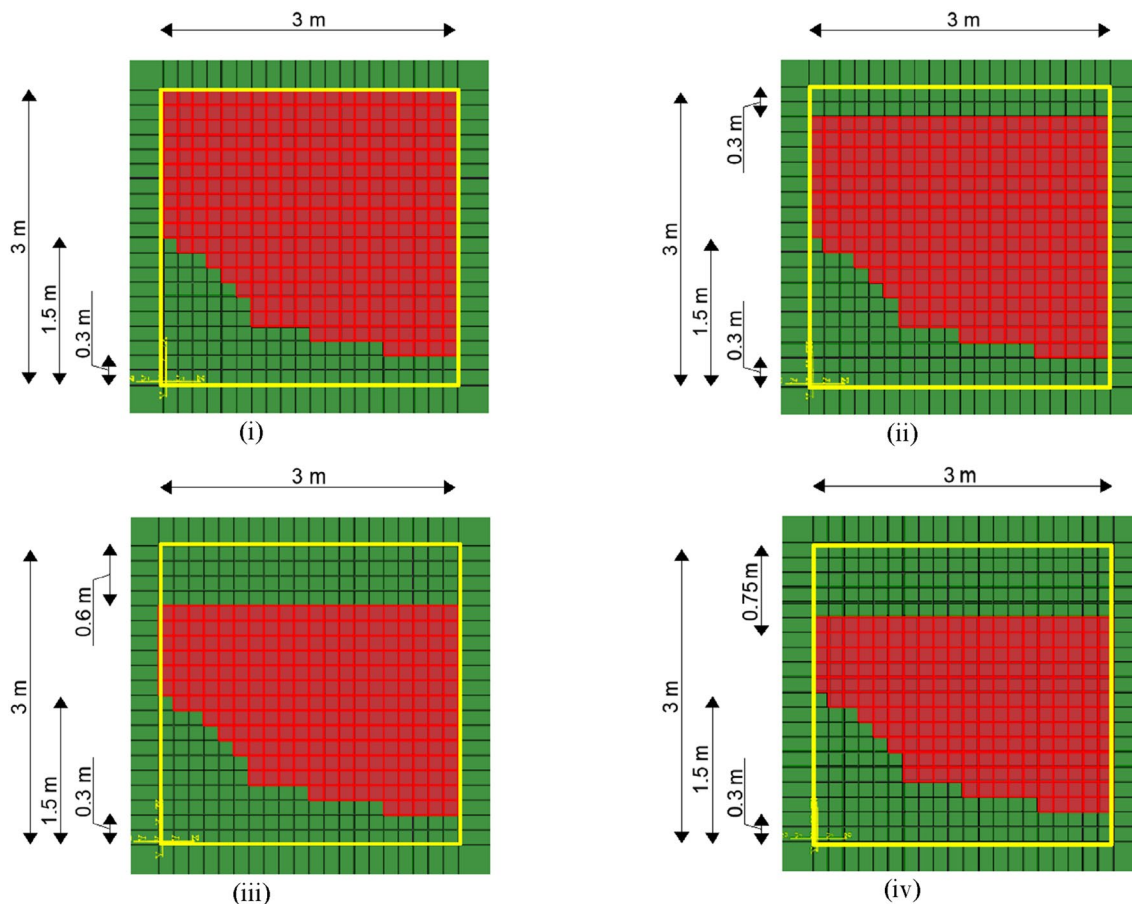


**Fig. 19** Contact area of soil–foundation interface for **i** the case of no scour and for scour width, **ii**  $S=0.3$  m, **iii**  $S=0.6$  m and **iv**  $S=0.75$  m

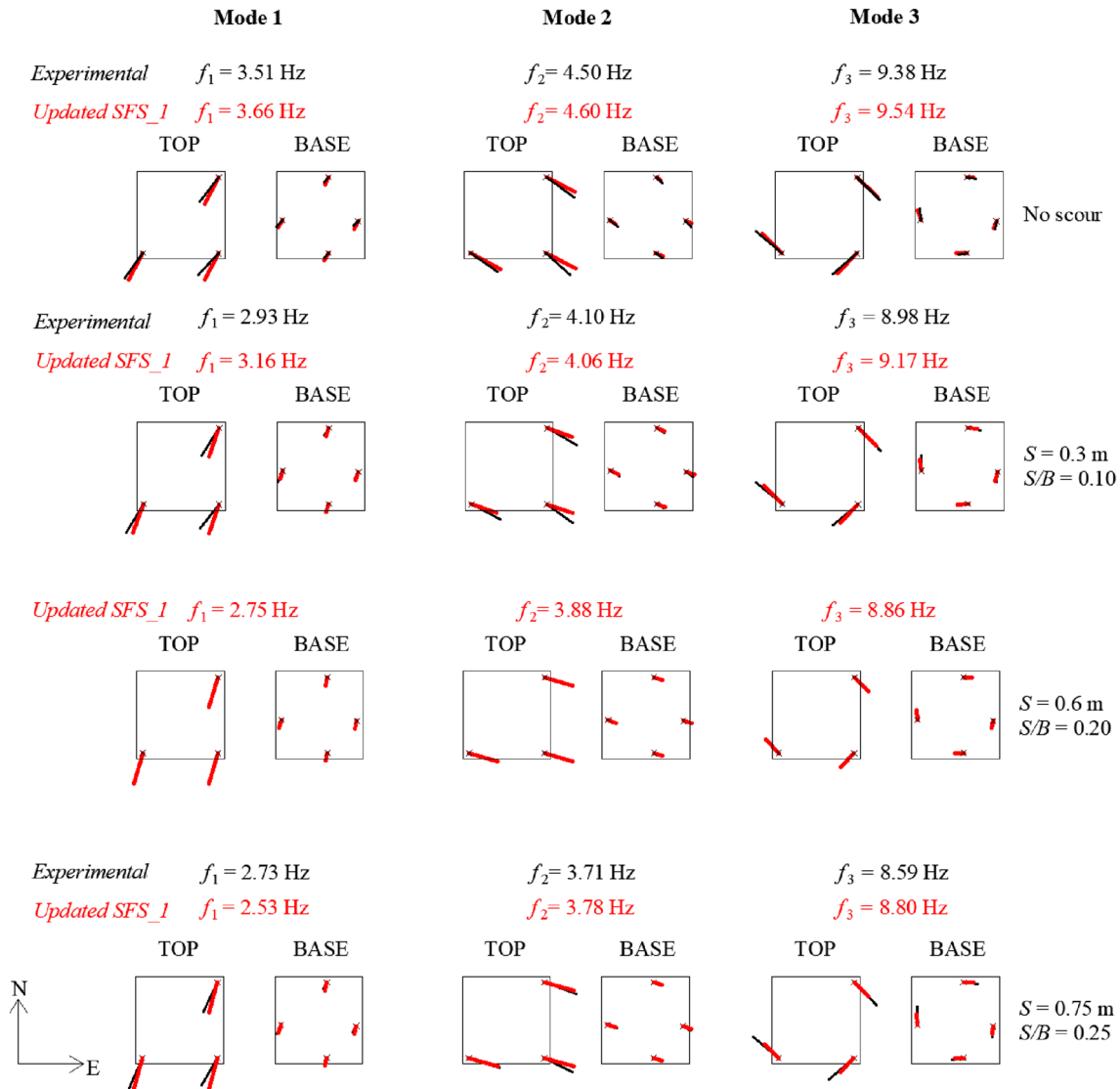


**Fig. 20** Numerical modal shapes for system with no scour, and normalised scour widths  $S/B=0.1$  m,  $S/B=0.2$  m and  $S/B=0.25$  m. Plan view of top and base horizontal displacements

embedded depth of the foundation has some influence on the vibration frequency of the system and on the frequency reduction for increasing scour widths;

- the three dimensional modelling strategy, describing the soil as a continuum with absorbing boundaries, can provide very accurate estimates of the vibration modes and frequencies of the system for all the investigated scour scenarios, provided that the non-uniform contact between the soil and the foundation is modelled accurately.

These study results are very relevant for the development of strategies for monitoring bridges at risk of scour through vibration-based techniques. In this regard, it should be specified that the scour results in very different effects, in terms of change of vibration frequency, on different systems. For

**Table 5** MAC values between the experimental mode vectors and the matched numerical mode vectors

$S/B$	MAC		
	Mode 1	Mode 2	Mode 3
0	0.95	0.96	0.99
0.1	0.94	0.95	0.99
0.25	0.96	0.99	0.99

example, in the investigated case, characterised by a significant foundation rocking and a superstructure behaving linearly also for large scour widths, the frequency reduction due to scour is overall not very significant. In more complex

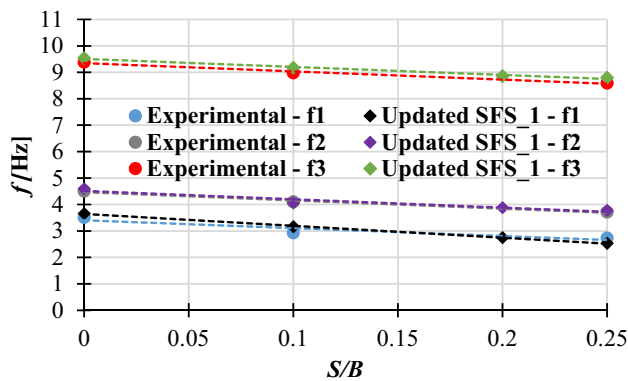


**Fig. 21** Variation of the vibration frequencies of the monitored modes with the normalized scour width  $S/B$  derived by the updated SFS\_1 model and experiments

structural systems with the superstructure behaving non-linearly due to damage and cracking even under moderate levels of scour, as in the case of masonry arch bridges, the frequency reduction is expected to be even more significant in comparison to the investigated case.

Finally, the experimental results and interpretation of the force–vibration tests will be the object of future studies, which will also investigate the influence of scour on the kinematic and inertial interaction of bridges with scoured shallow foundations under seismic input, by considering more realistic soil profile scenarios and bridge configurations. Future studies will also investigate further the effects of scour on EuroProteas structure for higher scour widths by assuming a non-linear soil behavior, where non-linear phenomena are expected to be significant. These results will be used to inform the design and assessment of bridges subjected to scour and earthquake hazards, and will provide evidence for the development of the next generation of Eurocode 8–2.

**Acknowledgements** This study was performed in the framework of the Transnational Access Project “Soil Frame-Interaction Analysis through large-scale tests and advanced numerical finite element modeling” funded under the European project “Seismology and Earthquake Engineering Research Infrastructure Alliance for Europe—SERA-TA-H2020 (Grant Agreement 730900)”.

**Open Access** This article is licensed under a Creative Commons Attribution 4.0 International License, which permits use, sharing, adaptation, distribution and reproduction in any medium or format, as long as you give appropriate credit to the original author(s) and the source, provide a link to the Creative Commons licence, and indicate if changes were made. The images or other third party material in this article are included in the article's Creative Commons licence, unless indicated otherwise in a credit line to the material. If material is not included in the article's Creative Commons licence and your intended use is not permitted by statutory regulation or exceeds the permitted use, you will need to obtain permission directly from the copyright holder. To view a copy of this licence, visit <http://creativecommons.org/licenses/by/4.0/>.

## References

- Melville BW, Coleman SE (2000) Bridge scour. Water Resources Publications, Highlands Ranch
- Pizarro A, Manfreda S, Tubaldi E (2020) The science behind scour at bridge foundations: a review. *Water* 12(20):74. <https://doi.org/10.3390/w12020374>
- Imam B (2019) Climate change impact for bridges subjected to scour and corrosion. In: *Climate adaptation engineering*. Butterworth-Heinemann, pp 165–206
- Assessing scour risk on bridges (2013) Innovation and research focus issue no. 93
- Zekkos D, Zalachoris G, Alvertos AE, Amatya PM, Blunts P, Clark M et al (2020) The September 18–20 2020 Mediane Ianos Impact on Greece—Phase I Reconnaissance Report. Geotechnical Extreme Events Reconnaissance Report, GEER-068. <https://doi.org/10.18118/G6MT1T>
- Tubaldi E, Macorini L, Izzuddin BA (2018) Three-dimensional mesoscale modelling of multi-span masonry arch bridges subjected to scour. *Eng Struct* 165:486–500. <https://doi.org/10.1016/j.engstruct.2018.03.031>
- Tubaldi E, Macorini L, Izzuddin BA, Manes C, Laio F (2017) A framework for probabilistic assessment of clear-water scour around bridge piers. *Struct Saf* 69:11–22. <https://doi.org/10.1016/j.strusafe.2017.07.001>
- Pizarro A, Tubaldi E (2019) Quantification of modelling uncertainties in bridge scour risk assessment under multiple flood events. *Geosciences* 9:445. <https://doi.org/10.3390/geosciences9100445>
- Argyroudis SA, Mitoulis SA (2021) Vulnerability of bridges to individual and multiple hazards—floods and earthquakes. *Reliab Eng Syst Saf* 210:107564. <https://doi.org/10.1016/j.res.2021.107564>
- Mitoulis SA, Argyroudis SA, Loli M, Imam B (2021) Restoration models for quantifying flood resilience of bridges. *Eng Struct* 238:112180. <https://doi.org/10.1016/j.engstruct.2021.112180>
- Ko YY, Chiou JS, Tsai YC, Chen CH, Wang H, Wang CY (2014) Evaluation of flood-resistant capacity of scoured bridges. *J Perform Constr Facil* 28(1):61–75. [https://doi.org/10.1061/\(ASCE\)CF.1943-5509.0000381](https://doi.org/10.1061/(ASCE)CF.1943-5509.0000381)
- Prendergast LJ, Gavin K (2014) A review of bridge scour monitoring techniques. *J Rock Mech Geotech Eng* 6(2):138–149. <https://doi.org/10.1016/j.jrmge.2014.01.007>
- Kirby AM, Roca M, Kitchen A, Escarameia M, Chesterton OJ (2015) Manual on scour at bridges and other hydraulic structures, 2nd edn. CIRIA, C742, London
- Tubaldi E, White CJ, Patelli E, Mitoulis SA, De Almedia G, Brown J et al (2022) Invited perspectives: challenges and future direction in improving bridge flood resilience. *Nat Hazards Earth Syst Sci* 22:795–812. <https://doi.org/10.5194/nhess-22-795-2022>
- Crotti G, Cigada A (2019) Scour at river bridge piers: real-time vulnerability assessment through the continuous monitoring of a bridge over the river Po, Italy. *J Civ Struct Health Monit* 9:513–528. <https://doi.org/10.1007/s13349-019-00348-5>
- Briaud J, Hurlbaeus S, Chang K, Yao C, Sharma H, Yu OY et al (2011) Realtime monitoring of bridge scour using remote monitoring technology. Texas Department Institute, The Texas A&M University System. Report no. FHWA/TX-11/0-6060-1
- Prendergast LJ, Hester D, Gavin K, O’Sullivan JJ (2013) An investigation of the changes in the natural frequency of a pile affected by scour. *J Sound Vib* 332:6685–6702. <https://doi.org/10.1016/j.jsv.2013.08.020>
- Bao T, Swartz AR, Vitton S, Sun Y, Liu ZC (2017) Critical insights for advanced bridge scour detection using the natural

- frequency. *J Sound Vib* 386:116–133. <https://doi.org/10.1016/j.jsv.2016.06.039>
19. Foti S, Sabia D (2011) Influence of foundation scour on the dynamic response of an existing bridge. *J Bridge Eng* 16(2):295–304. [https://doi.org/10.1061/\(ASCE\)BE.1943-5592.0000146](https://doi.org/10.1061/(ASCE)BE.1943-5592.0000146)
  20. Prendergast LJ, Gavin K, Hester D (2017) Isolating the location of scour-induced stiffness loss in bridges using local modal behaviour. *J Civ Struct Health Monit* 7:483–503. <https://doi.org/10.1007/s13349-017-0238-3>
  21. Bao T, Liu ZL (2021) Bridge scour characteristic curve for natural frequency-based bridge scour monitoring using simulation-based optimization. *Struct Health Monit* 28(8):e2773. <https://doi.org/10.1002/stc.2773>
  22. Chen CC, Wu WH, Slih F, Wang SW (2014) Scour evaluation for foundation of a cable-stayed bridge based on ambient vibration measurements of superstructure. *NDT E Int* 66:16–27. <https://doi.org/10.1016/j.ndteint.2014.04.005>
  23. Xiong W, Cai CS, Kong B, Zhang X, Tang P (2019) Bridge scour identification and field application based on ambient vibration measurements of superstructures. *J Mar Sci Eng* 7(5):121. <https://doi.org/10.3390/jmse7050121>
  24. Kim CW, Yoshitome K, Goi Y, Zhang FL, Kitagawa S, Shinoda M et al (2019) Scour detection of railway bridges by microtremor monitoring. In: Proceedings of the 16th East Asia-Pacific conference on structural engineering and construction (EASEC16). Springer, pp 97–107
  25. Kariyawasam KKGKD, Fidler PRA, Talbot JP, Middleton CR (2019) Field deployment of an ambient vibration-based scour monitoring system at Baildon Bridge, UK. In: International conference on smart infrastructure and construction (ICSIC), Cambridge, pp 711–719. <https://doi.org/10.1680/icsic.64669.711>
  26. Lee SO, Abid I, Hong SH (2021) Effect of complex shape of pier foundation exposure on time development of scour. *Environ Fluid Mech* 21:103–127. <https://doi.org/10.1007/s10652-020-09765-3>
  27. Federico F, Silvagni G, Volpi F (2003) Scour Vulnerability of River Bridge Piers. *Geotech Geoenviron Eng* 129:10. [https://doi.org/10.1061/\(ASCE\)1090-0241\(2003\)129:10\(890\)](https://doi.org/10.1061/(ASCE)1090-0241(2003)129:10(890))
  28. Kariyawasam KD, Campbell R, Madabhushi G, Haigh SK, Talbot JP (2020) Assessment of bridge natural frequency as an indicator of scour using centrifuge modelling. *J Civ Struct Health Monit* 10:861–881. <https://doi.org/10.1007/s13349-020-00420-5>
  29. Malekjafarian A, Kim C, O'Brien EJ, Prendergast LJ, Fitzgerald PC, Nakajima S (2020) Experimental demonstration of a mode shape-based scour-monitoring method for multispan bridges with shallow foundations. *J Bridge Eng* 25(8):04020050. [https://doi.org/10.1061/\(ASCE\)BE.1943-5592.0001586](https://doi.org/10.1061/(ASCE)BE.1943-5592.0001586)
  30. Zampieri P, Zanini MA, Faleschini F, Hofer L, Pellegrino C (2017) Failure analysis of masonry arch bridges subject to local pier scour. *Eng Fail Anal* 79:371–384. <https://doi.org/10.1016/j.engfailanal.2017.05.028>
  31. Tanasić N, Hajdin R (2017) Management of bridges with shallow foundation exposed to local scour. *Struct Infrastruct Eng* 14(4):468–476. <https://doi.org/10.1080/15732479.2017.1406960>
  32. Guo X (2014) Seismic vulnerability analysis of scoured bridge systems. PhD Thesis, University of Missouri-Kansas City
  33. Ruocci G, Quattrone A, Fragonara ZL, Ceravolo R, De Stefano A (2011) Experimental testing of a masonry arch bridge model subject to increasing level of damage. In: Proceedings of 4th international conference on advances in experimental structural engineering. ISPRA, Lombardy
  34. Scozzese F, Ragni L, Tubaldi E, Gara F (2019) Modal properties variation and collapse assessment of masonry arch bridges under scour action. *Eng Struct* 199:109665. <https://doi.org/10.1016/j.engstruct.2019.109665>
  35. DYMOBRIS EU Project. <http://www.infrastructuresilience.com/dymobris/>
  36. Pitilakis D, Rovithis E, Anastasiadis A, Vratisikidis A, Manakou M (2018) Field evidence of SSI from full-scale structure testing. *Soil Dyn Earthq Eng* 112:89–106. <https://doi.org/10.1016/j.soildyn.2018.04.024>
  37. Vratisikidis A, Pitilakis D, Anastasiadis A, Kapouniaris A (2021) Evidence of soil-structure interaction from modular full-scale field experimental tests. *Bull Earthq Eng*. <https://doi.org/10.1007/s10518-021-01286-8>
  38. Wang X, Ji B, Ye A (2020) Seismic behavior of pile-group-supported bridges in liquefiable soils with crusts subjected to potential scour: insights from shake-table tests. *J Geotech Geoenviron Eng* 146(5):04020030. [https://doi.org/10.1061/\(asce\)gt.1943-5606.0002250](https://doi.org/10.1061/(asce)gt.1943-5606.0002250)
  39. Prasad GG, Banerjee S (2013) The impact of flood-induced scour on seismic fragility characteristics of bridges. *J Earthq Eng* 17(6):803–828. <https://doi.org/10.1080/13632469.2013.771593>
  40. He H, Wei K, Zhang J, Qin S (2020) Application of endurance time method to seismic fragility evaluation of highway bridges considering scour effect. *Soil Dyn Earthq Eng* 136(11):106243. <https://doi.org/10.1016/j.soildyn.2020.106243>
  41. Shang Y, Alipour A, Ye A (2018) Selection of input motion for seismic analysis of scoured pile-supported bridge with simplified models. *J Struct Eng* 144(8):04018099. [https://doi.org/10.1061/\(asce\)st.1943-541x.0002067](https://doi.org/10.1061/(asce)st.1943-541x.0002067)
  42. Fioklou A, Alipour A (2019) Significance of non-uniform scour on the seismic performance of bridges. *Struct Infrastruct Eng* 15(6):822–836. <https://doi.org/10.1080/15732479.2019.1584226>
  43. Manakou MV, Raptakis DG, Chávez-García FJ, Apostolidis PI, Pitilakis KD (2010) 3D soil structure of the Mygdonian basin for site response analysis. *Soil Dyn Earthq Eng* 30(11):1198–1211. <https://doi.org/10.1016/j.soildyn.2010.04.027>
  44. Raptakis D, Theodulidis N, Pitilakis K (1998) Data analysis of the euroseistest strong motion array in Volvi (Greece): standard and horizontal-to-vertical spectral ratio techniques. *Earthq Spectra* 14(1):203–224. <https://doi.org/10.1193/1.1585996>
  45. Raptakis D, Chávez-García F, Makra K, Pitilakis K (2000) Site effects at EuroSeistest-I. Determination of the valley structure and confrontation of observations with 1D analysis. *Soil Dyn Earthq Eng* 19(1):1–22. [https://doi.org/10.1016/S0267-7261\(99\)00025-1](https://doi.org/10.1016/S0267-7261(99)00025-1)
  46. Pitilakis K, Raptakis D, Lontzetidis K, Tika-Vasilikou T, Jongmans D (1999) Geotechnical and geophysical description of EUROSEISTEST, using field, laboratory tests and moderate strong motion records. *J Earthq Eng* 3(3):381–409. <https://doi.org/10.1080/13632469909350352>
  47. Abaqus V. 6.14 Documentation (2014) Dassault Systemes Simulia Corporation
  48. MATLAB and Statistics Toolbox Release 2012b. The MathWorks, Inc., Natick
  49. Antonopoulos C, Tubaldi E, Carbonari S, Gara F, Dezi F (2022) Dynamic behaviour of soil-foundation-structure systems subjected to scour. *Soil Dyn Earthq Eng* 152:106969. <https://doi.org/10.1016/j.soildyn.2021.106969>
  50. Seismic Engineering Research Infrastructures for European Synergies (2012) Report on field testing for assessing input motion and SSI, Project No.: 227887
  51. Kuhlemeyer RL, Lysmer J (1973) Finite element method accuracy for wave propagation problems. *J Soil Mech Found Div* 99:421–427
  52. Gazetas G (1991) Formulas and charts for impedances of surface and embedded foundations. *J Geotech Eng* 117(9):1363–1381
  53. Wolf JP (1989) Soil-structure-interaction analysis in time domain. *Nucl Eng Des* 111:381–393. [https://doi.org/10.1016/0029-5493\(89\)90249-5](https://doi.org/10.1016/0029-5493(89)90249-5)
  54. Hryniewicz Z (1981) Dynamic response of a rigid strip on an elastic half-space. *Comput Methods Appl Mech Eng* 25(3):355–364. [https://doi.org/10.1016/0045-7825\(81\)90038-4](https://doi.org/10.1016/0045-7825(81)90038-4)

55. Tileylioglu S, Stewart JP, Nigbor RL (2010) Dynamic stiffness and damping of a shallow foundation from forced vibration of a field test structure. *J Geotech Geoenvironmental Eng* 137(4):344–353. [https://doi.org/10.1061/\(ASCE\)GT.1943-5606.0000430](https://doi.org/10.1061/(ASCE)GT.1943-5606.0000430)
56. Brincker R, Zhang L, Andersen P (2001) Modal identification of output-only systems using frequency domain decomposition. *Smart Mater Struct* 10(3):441. <https://doi.org/10.1088/0964-1726/10/3/303>
57. Pastor M, Binda M, Harcaric T (2012) Modal assurance criterion. *Procedia Eng* 48:543–548. <https://doi.org/10.1016/j.proeng.2012.09.551>

**Publisher's Note** Springer Nature remains neutral with regard to jurisdictional claims in published maps and institutional affiliations.